

VibrantVS: A High-Resolution Multi-Task Transformer for Forest Canopy Height Estimation

Tony Chang¹, Kiarie Ndegwa¹, Andreas Gros^{1*},
 Vincent A. Landau¹, Luke J. Zachmann¹, Bogdan State¹, Mitchell A. Gritts¹,
 Colton W. Miller¹, Nathan E. Rutenbeck¹, Scott Conway¹, and Guy Bayes¹

¹ Vibrant Planet Public Benefit Corporation
 11025 Pioneer Trail Unit 206 Truckee, CA, USA

Abstract

This paper explores the application of a novel multi-task vision transformer (ViT) model for the estimation of canopy height models (CHMs) using 4-band National Agriculture Imagery Program (NAIP) imagery across the western United States. We compare the effectiveness of this model in terms of accuracy and precision aggregated across ecoregions and class heights versus three other benchmark peer-reviewed models. Key findings suggest that, while other benchmark models can provide high precision in localized areas, the VibrantVS model has substantial advantages across a broad reach of ecoregions in the western United States with higher accuracy, higher precision, the ability to generate updated inference at a cadence of three years or less, and high spatial resolution. The VibrantVS model provides significant value for ecological monitoring and land management decisions, including for wildfire mitigation.

Keywords: canopy height model · computer vision · lidar · remote sensing · forest structure

1 Introduction

During the past three decades, increases in the number of wildfires and burned areas across the western United States have negatively impacted human health, assets, and ecological structure and function [30, 56]. This fire activity, compounded by recent widespread drought and historic fire suppression [1], has led to forest conditions that lack sufficient resilience to recover from natural disturbances and thereby threatens the ecosystem services on which human communities depend [18, 43]. Such conditions have required forest managers to prioritize the restoration of historical fire regimes and the treatment and maintenance of forests to reduce the potential for high-severity fire [19]. A major requirement in the identification of appropriate treatments and restoration actions is access to current spatial data that accurately describes the horizontal and vertical structure of vegetation.

*Corresponding author: andi@vibrantplanet.net

Canopy height models (CHMs) describe the height of the canopy top from the ground. The availability of current canopy height data in a three-dimensional georeferenced surface [52] is crucial for various ecological applications including biomass estimation [28], predicting fire behavior [3, 35] individual tree detection [33, 41], and habitat quality assessment [53]. Accurate quantification of canopy height not only enhances our understanding of forest dynamics [5, 24, 58], but also facilitates strategic, tactical, and operational planning decisions to improve forest health, promote biodiversity, and protect threatened and endangered species [57]. Therefore, the development of a high resolution continuous CHM across large (in excess of 1 million ha), multi-jurisdictional landscapes such as the western United States is critical for the successful restoration, monitoring, and management of forests.

Lidar data has emerged as the gold standard for three-dimensional mapping of vegetation structure due to its high spatial fidelity and ability to penetrate forest canopies [21, 24, 31]. However, even with economies of scale [17] and cost effectiveness compared to conducting field inventories over large areas [28], lidar datasets are constrained by their limited spatial and temporal coverage. These constraints limit the ability of lidar acquisitions to reflect up-to-date forest structure because of the dynamic nature of forest ecosystems as they respond to disturbances, treatments, natural growth, or climate change [13]. On the other hand, the proliferation of freely available, remotely sensed data with consistent temporal revisit periods, such as the satellite-based imagery of Sentinel-2 [11], or aerial imagery from NAIP, has opened new avenues to methodologies that can be tailored to model vegetation structure with high spatial and temporal resolution over longer periods of time and over larger areas [51, 54].

The availability of large remotely sensed image libraries in conjunction with newer deep learning methods has allowed for the emergence of a suite of modeled canopy height products providing continuous high resolution (1m-30m) forest structure measurements across broad spatial extents [23, 25, 47]. This paper aims to benchmark a selection of the latest peer-reviewed deep learning/machine learning-based CHMs across varied ecosystems in the western United States. Additionally, we describe our own multi-task vision transformer model based on NAIP imagery: VibrantVS. We present an analysis that will: 1) address which model is optimal based on standard machine learning metrics compared to aerial lidar measurements to serve as a benchmark for the broad remote sensing community; and 2) compare model estimates across a variety of ecoregions in the western United States to better understand the utility of these models for fine-grained ecological management and decision making.

2 Study Area and Data

In this study, we compare CHMs for the western contiguous United States. Given our focus on forest structure data that would have the greatest utility in understanding wildfire impacts, we focus our sampling to intersect (Fig. 1):

1. The Wildfire Crisis Strategy (WCS) landscapes defined by the United States Forest Service (USFS) to prioritize regions at the greatest risk of severe wildfire. [48].
2. National Ecological Observatory Network (NEON) research sites within the western United States, due to their independent collection of individual field-based tree height measurements and aerial lidar against which to validate model predictions [46].

3. Areas that intersect the spatial extent for the 3D Elevation Program (3DEP) work units in the Work Unit Extent Spatial Metadata (WESM) dataset [50] that meet the seamless and 1-meter DEM quality criteria.

To quantify the ability of the models to robustly predict forest canopy height across an ecological gradient, we stratify our data by Environmental Protection Agency (EPA) Level 3 (L3) ecoregions [32]. EPA L3 ecoregions are delineated based on relatively homogeneous environmental conditions, such as vegetation types, soil, climate, and landforms. This coherence reduces variability in environmental factors unrelated to canopy height within each ecoregion, making it easier to evaluate the performance of the baseline models across a well-defined set of environmental conditions. Additionally, EPA L3 ecoregions provide a manageable range of dominant species and climate variability while still capturing key regional distinctions. Finally, evaluating CHM performance at this ecoregion scale can directly inform practices in forest management, carbon accounting, and biodiversity conservation.

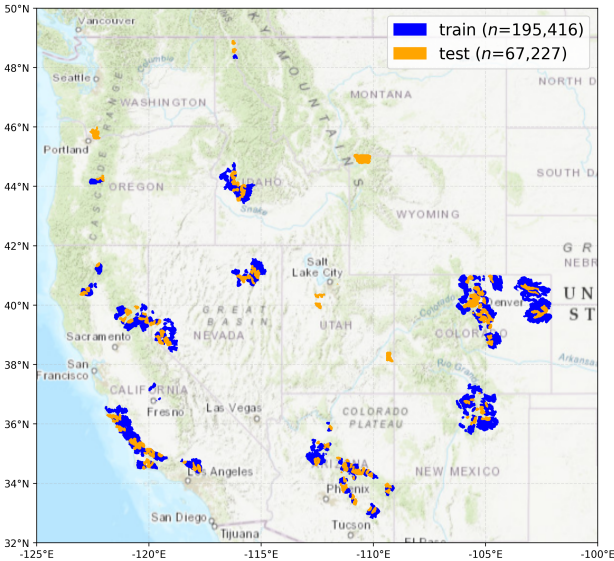


Figure 1: Sampling of tiles within Hydrologic Units 12 (HUC12) watersheds of the western United States that covers 24 EPA L3 ecoregions containing sufficient quality 3DEP lidar data and spatially/temporally intersecting NAIP data. Regions were additionally selected within WCS areas to optimize for model evaluation in regions where wildfire risk mitigation is a priority.

We generated a total of 262,643 sample tiles with a spatial footprint of $0.5 \times 0.5 \text{ km}^2$ ($1,000 \times 1,000$ pixel rasters at 0.5-meter resolution) that crossed a total of 24 different EPA L3 ecoregions (Fig.2), providing us with a robust representation of tree vegetation data and lidar CHM heights (Fig.A1). We split the data into two groups: 1) a ‘train’ set of 195,416 samples, which contains data for training and validation of the VibrantVS ViT model; and 2) a test set of 67,227 samples, which contain tiles withheld from the model to evaluate performance. The lidar collection dates range from 2014 to 2021 (Table 1).

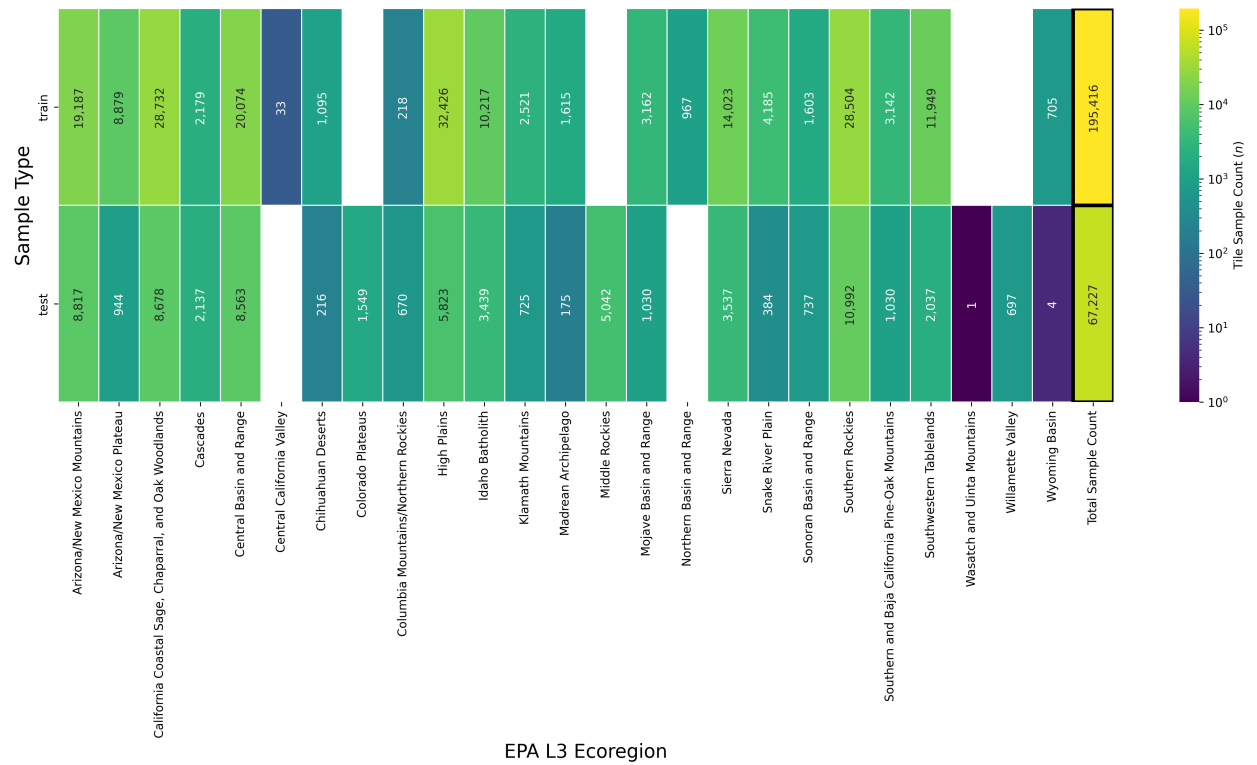


Figure 2: Sample tile counts within each of the randomly sampled train and test (approx. 85% to 15% ratio) groups by EPA L3 ecoregion.

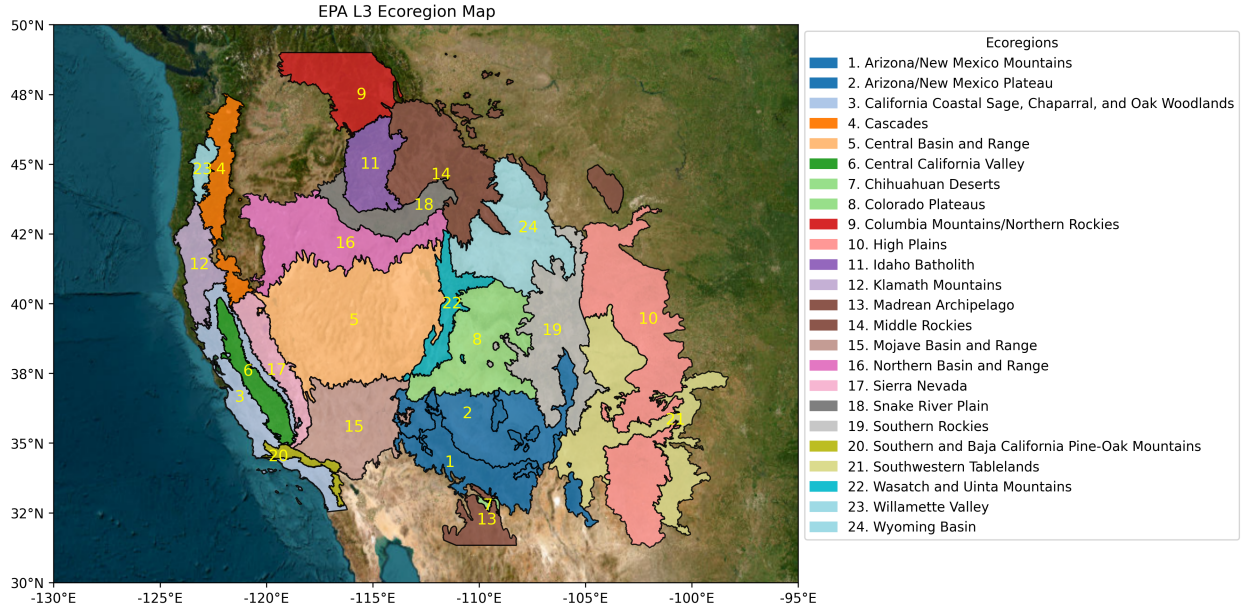


Figure 3: Map of EPA L3 Ecoregions into which our test tiles were aggregated to evaluate baseline model performance.

e

2.1 Predictor Data

2.1.1 NAIP Imagery

We utilized 4-band NAIP imagery, which includes RGB and near-infrared (NIR) bands [14]. NAIP data are collected at the state level in varying temporal frequencies (originally at five-year cycles and every three years or less since 2009) and at varying spatial resolutions from 0.3 meters to 1 meter since the year 2002 to the present. To create uniform training, test, and inference datasets we collected data from the AWS Open Data Registry [4] and resampled the NAIP data to a common spatial resolution of 0.5 meters using a bilinear interpolation for the years of 2014-2022. We tiled the NAIP data into $1 \times 1 \text{ km}^2$ spatial footprint tiles and stored them within AWS S3 storage buckets in Cloud-Optimized GeoTIFF format. We filtered NAIP tile data to be within one year of the spatially coincident lidar acquisition date to reduce opportunities for incorrect labels for the same tile due to disturbances such as wildfires.

2.2 Label Data

2.2.1 3DEP Lidar

We downloaded available lidar data developed by the USGS 3DEP program [44]. All lidar geospatial metadata is available by work unit in the Work Unit Extent Spatial Metadata (WESM) GeoPackage that is published daily [50]. The WESM contains information about lidar point clouds and which source digital elevation model (DEM) work units have been processed and made available to the public. It includes metadata about work units, including quality level, data acquisition dates, and links to project-level metadata. We developed automated scripts to download raw ‘laz’ files from

Table 1: Summary of samples by lidar collection year and unique EPA L3 ecoregions. Sample tiles are $1 \times 1 \text{ km}^2$, so n samples is also the total area in (km^2).

Train		
Lidar acq. year	n samples	# unique ecoregions
2014	523	2
2015	6,568	2
2016	24,838	7
2017	32,880	8
2018	54,114	11
2019	24,974	11
2020	44,003	6
2021	7,516	6
Test		
Lidar acq. year	n samples	# unique ecoregions
2015	1,384	2
2016	7,966	6
2017	9,616	7
2018	13,747	12
2019	8,748	9
2020	22,459	7
2021	3,307	6

the associated download URLs. We used the ‘lidR’ package in R [39] to process the data as follows:

1. download, reproject, tile raw lidar data
2. create outlier filtered normalized point clouds
3. create Digital Terrain Models (DTM)
4. create Digital Surface Models (DSM)
5. create Canopy Height Models (CHM)

These processed lidar assets are stored in $0.5 \times 0.5 \text{ km}^2$ tiles within our AWS S3 storage buckets in Cloud-Optimized GeoTIFF format at a 0.5-meter pixel size ($1,000 \times 1,000$ pixels).

2.3 Baseline Evaluation Data

In this study we evaluate data from three existing forest canopy height models as a baseline in comparison to the VibrantVS model. In order to have greater uniformity in the data, all baseline model outputs were resampled to a 0.5-meter resolution with nearest neighbor resampling and tiled into $1 \times 1 \text{ km}^2$ spatial footprint tiles.

2.3.1 Meta Data For Good (Meta) High Resolution Canopy Height - DINOv2 Architecture

To assess the benefit of the self-supervised training phase on satellite data, we use output data from Meta’s state-of-the-art DINOv2 vision encoder as baseline CHM data [47]. Meta’s approach consists of three different models trained in separate stages, namely an encoder, a dense prediction transformer, and a correction and rescaling network. Four different datasets are used: Maxar Vivid2 0.5-meter resolution mosaics [27], NEON aerial lidar surveyed CHMs, Global Ecosystem Dynamics Investigation (GEDI) data and a labeled 9000 tile tree/no tree segmentation dataset [12]. At the time of writing this manuscript, this model was one of the only global CHMs with documented performance at 1-meter spatial resolution for the year representing 2020. We downloaded these data provided by the World Resources Institute, which are stored on AWS [29], for analysis.

2.3.2 LANDFIRE Forest Canopy Height model

The Landscape Fire and Resource Management Planning Tools (LANDFIRE) Project is a program developed to map the characteristics of wildland fuels, vegetation, and fire regime in the United States since 2001 [38]. Due to the national scope and complete spatial coverage across the entire United States, the LANDFIRE fuels dataset is a standard data input in North American fire models [22, 42, 55]. In this study, we compare the LANDFIRE Forest Canopy Height (FCH) dataset with lidar estimates. The LANDFIRE FCH layer uses regression-tree-based methods to model the relationships between field-measured height with spectral information from Landsat, as well as landscape feature information such as topography and biophysical gradient layers [37]. We collected this data from the LANDFIRE data portal for the year 2020 [49].

2.3.3 ETH Global canopy height model

The Lang et al. (2023) multi-modal model is a deep learning ensemble. This ensemble was trained using a multi-modal set of data, namely 10-meter resolution Sentinel-2-L2A multi-spectral images, sine-cosine embeddings of longitudinal coordinates, and sparse GEDI lidar data. These input data are used to model canopy top height and variance.

Model inference in this ETH model represents the year 2020 and all tiles were downloaded from the ETH Zurich library catalog and repository system [15].

3 Methodology

3.1 Vibrant Planet multi-task vegetation structure ViT: VibrantVS

The VibrantVS model consists of three main components: a base model and two heads. The base model employs an encoder-decoder Vision Transformer (ViT) architecture, while the heads are a metric-bin module head [6] and a light-weight convolution head. The encoder is derived from a modified version of the SWINv2 model [26], while the decoder uses a dense prediction transformer (DPT) [34] (Fig. 4). The DPT module processes features generated by the encoder to produce a normalized relative depth map. These features, along with dense features from the encoder via skip connections, are subsequently input into the metric-bin module head to predict canopy height and into the convolutional prediction head to predict canopy cover (CC).

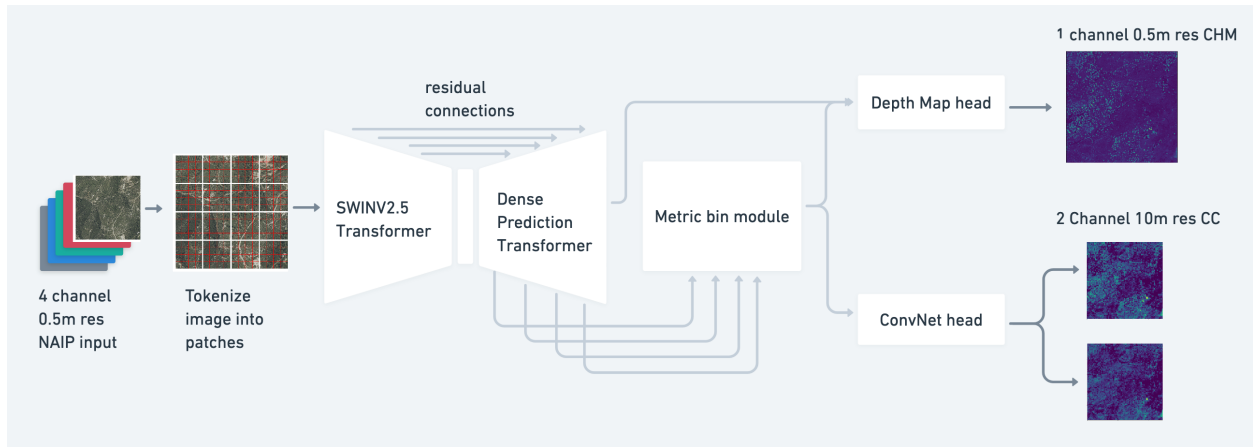


Figure 4: VibrantVS multi-task vision transformer architecture with 4 band NAIP input to predict CHM and CC.

The metric-bin module head learns the height distribution for each pixel, represented by 64 bins. These bins are linearly combined to generate dense features that are subsequently merged with feature tensors from the encoder through residual layers. The final output provides tree height metrics at a resolution of 0.5 meters and canopy cover at a resolution of 10 meters. Note that although this model produces both CHM and CC, we only evaluated the CHM portion in this research.

VibrantVS uses a custom modified version of SWINv2 to incorporate the latest transformer-architecture advancements, including token registers, as described in [8], this stabilized training and reduced noise in latent-attention features. Furthermore, we reconfigured the attention module to employ grouped query attention [2], Flash Attention V2 [7], and SWIGLU [40] activation with RMSNORM [59]. These modifications result in reduced training time and improved model convergence stability.

Certain recent optimization techniques, such as schedule-free optimization [9], did not converge effectively. However, the 8-bit Adam optimizer [10] demonstrated satisfactory performance and accelerated training compared to the traditional float32-based AdamW optimizer.

We extended the inference context window from 384x384 pixels to 1,536x1,536 pixels, enabling the model to produce more consistent and artifact-free outputs when handling NAIP inputs of varying quality, including optical artifacts such as seam lines resulting from the merging of data from different flight paths.

The model was trained end to end in a multi-task learning setting to predict both canopy height and canopy cover. Empirical results indicated that L1 loss outperformed Sigloss, providing improved training stability while requiring fewer learnable hyperparameters. The model was trained using input NAIP tiles, paired with dense canopy height data at a 0.5-meter resolution and canopy cover data at a 10-meter resolution. The dataset, approximately 10 terabytes in size, required 2,688 hours of training on an Nvidia 80GB A100 GPU.

To mitigate tiling checkerboard artifacts during inference, the ‘PyTorch’ functions ‘fold’ and ‘unfold’ were replaced with an in-memory buffer cache that makes use of memory pointers. This optimization facilitates the seamless merging of multiple inferences across tiles much larger than the model’s context window, enabling inference over regions up to $100,000 \times 100,000$ pixels using a

single Nvidia 24GB A10G GPU.

We summarize VibrantVS and the baseline models (Meta, LANDFIRE, and ETH) in Table A1.

3.2 Calculating error metrics

We applied a number of error metrics to all baseline models to evaluate the performance of the CHMs that include mean absolute error (MAE), coefficient of determination (R^2), Block- R^2 , root mean squared error (RMSE), mean absolute percent error (MAPE), mean error (ME), and edge error metric (EE) (see Appendix for error metric equations). These metrics were applied to VibrantVS and the baseline models after masking lidar CHM pixels < 2 meters in order to only include pixels that have a high potential to represent trees or higher vegetation. This reduced noise from low-lying vegetation or surface features that are not relevant for our canopy height study [16]. We also masked out lidar pixels where there were no data due to incomplete test tiles that may border flight path edges. To apply our error metrics, we spatially intersected all lidar CHM test tiles (500×500 -meter² area; $1,000 \times 1,000$ pixels at 0.5-meter spatial resolution) with VibrantVS and the baseline model CHMs. We then calculated the pixel-wise error metric across all 1,000,000 pixels in the test tile, accounting for all masked pixels. We repeated this for all test tiles and took the median error metric across tiles aggregated by:

1. The majority spatial intersection of tiles with the corresponding EPA L3 ecoregion to determine ecoregion-level accuracies.
2. Individual height bins within each tile to determine height-class accuracies.

4 Results

VibrantVS outperforms all baseline models with an overall median MAE of 2.71 meters, Meta: 4.83 meters; LANDFIRE: 5.96 meters; and ETH: 7.05 meters (Table 2). The overall mean error results show a median underestimation of canopy heights of 1.11 meters by VibrantVS, 4.03 meters by Meta, and a median overestimation by LANDFIRE of 0.92 meters and by the ETH model of 5.65 meters (Table 2).

Furthermore, the VibrantVS model consistently demonstrates lower error ranges in nearly all ecoregions analyzed, as evidenced by the narrower box plot widths for this model (Fig. 5). This highlights the higher CHM accuracy of VibrantVS at the tile level.

The observed error of VibrantVS is consistently the lowest in desert and low-elevation ecoregions, where vegetation heights are typically below 10 meters in height, demonstrating high accuracy in shrub and grass systems. As shown in Figure 11, the error increases substantially in western forests where the 95th percentile of lidar heights is above 25 meters, suggesting taller long-lived trees such as coastal redwoods and cedars pose a substantial challenge for all baseline models and the VibrantVS model (Fig. 11, 5). This is reflected in the MAE map (Fig. 6b) where MAE increases within ecoregions where there are larger species of western trees (see Fig. A2 for canopy height box plots by ecoregion).

Finally, our evaluation shows that all four models tend to truncate tree heights above 50 meters, with ETH’s model performing best in this height range (Fig. 11, 7).

The mean-error results by canopy height bins show that VibrantVS has less bias than the other baseline models in the range of 2 to 25 meters. These height classes coincide with the majority of

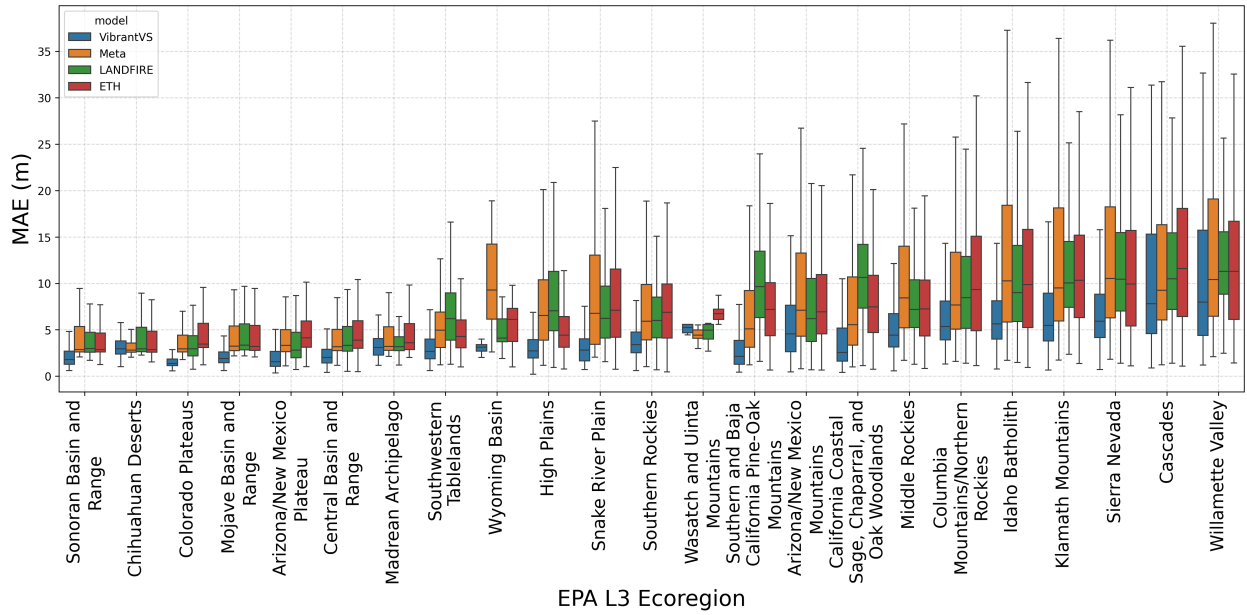


Figure 5: Box and whisker plots of test tile level MAE by model and ecoregion sorted by lowest to highest median MAE across all models.

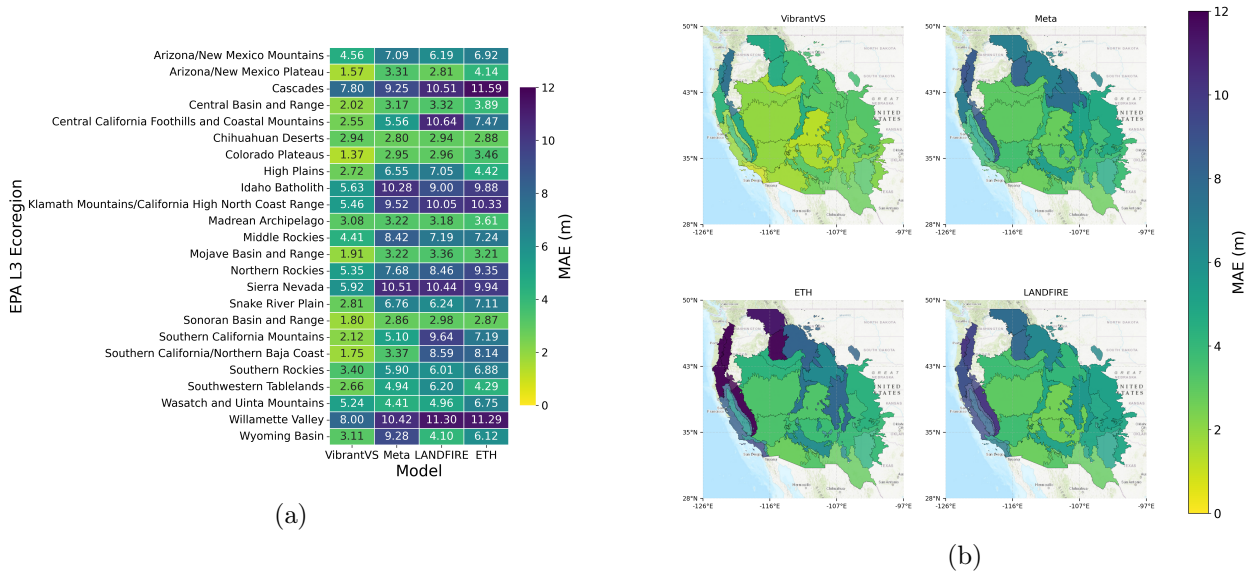


Figure 6: (a) Results of MAE by ecoregion within all test tiles. (b) Map of MAE by ecoregions within all validation and test tiles to give complete display of the spatial relationship of baseline model performance.

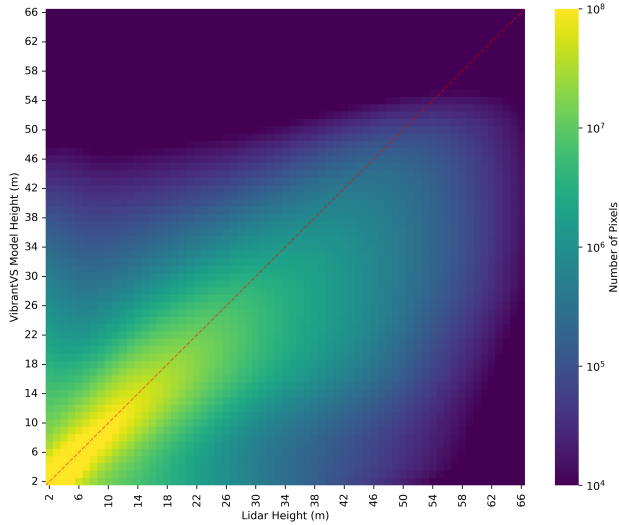


Figure 7: 2D histogram plot of VibrantVS canopy heights vs lidar-derived canopy heights across test samples.

the lidar pixels in our test data. Beyond these heights, LANDFIRE and ETH tend to outperform VibrantVS when compared to lidar (Fig. 8). However, while the VibrantVS and Meta models tend to show increasingly negative mean error at higher height bins, both LANDFIRE and ETH strongly overestimate lower canopy height bins.

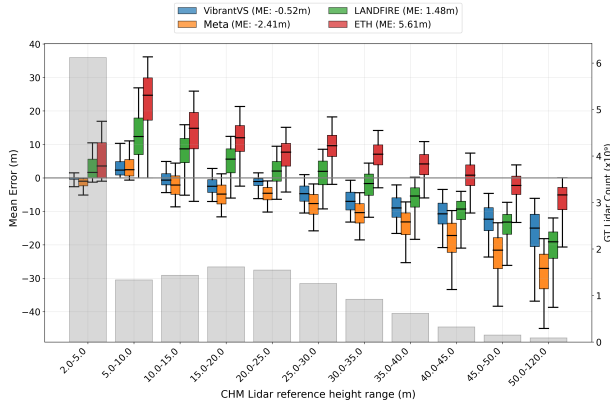


Figure 8: Box plots of mean error in different height bins and histogram of sample counts per height bin.

The summaries in Table 2 indicate that VibrantVS outperforms the other baseline models for mean absolute error (MAE), Block- R^2 , and edge error metrics, suggesting a better ability to synthesize lidar-like CHM outputs. The median Block- R^2 [47] numbers across all tiles also reflect the performance trend of MAE and ME (compare Table 2 and Fig. 9).

Table 2: Summary of baseline model across all test tiles for all error metrics.

Model Name	MAE	Mean Error	Block-R ²	Edge Error
VibrantVS	2.71	-1.11	0.69	0.08
Meta	4.83	-4.03	-0.60	0.30
LANDFIRE	5.96	0.92	-1.45	0.63
ETH	7.05	5.65	-1.85	0.64

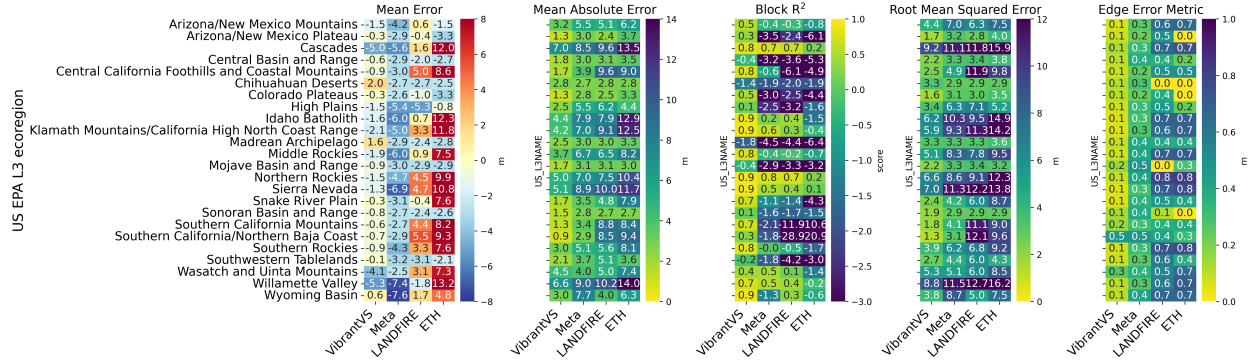


Figure 9: Comparison of model performance by ecoregion for every error metric.

4.1 Qualitative analysis

The Meta and VibrantVS CHM estimates provide finer resolution data that are visually closer to the corresponding aerial lidar data, resulting in higher fidelity for fine-scale applications (Fig. 10). This is made evident by the lower median edge errors (EE) observed for these models compared to ETH and LANDFIRE (see Appendix Eq. 5) between the models, where VibrantVS’s EE equals 0.08, compared to Meta with 0.3, and ETH and LANDFIRE at 0.63 and 0.64 (Table 2). Considering the coarser resolution of the LANDFIRE and ETH data, their estimates often result in a constant value and a general overestimation of the CHM values compared to lidar and a lower underestimation in canopy heights beyond 30 meters (Fig. 11). When we aggregate VibrantVS’s results to 10 and 30 meters and compare them with the baseline models at the same resolution, we find that the trends in differences between the overall median MAEs are consistent with the 0.5-meter results. (Fig.12).

5 Discussion

In this paper, we evaluate a novel vision transformer model against other baseline canopy height models. Our results demonstrate that the VibrantVS model produces a high-accuracy, high-precision CHM across ecoregions in the western United States.

The overall performance of the VibrantVS model is likely better than the baseline models because we use a larger quantity of training data from a broader set of ecoregions (Table 1, Fig. 2). Our training and test data are based on a CHM created from aerial lidar from a wide range of ecoregions in the western United States with a total surface area of 190,000 km², allowing our model to learn a wider range of landscape canopy-height patterns. In contrast, the baseline models were trained on more limited regions: NEON sites, Forest Inventory and Analysis (FIA) field plots, or select

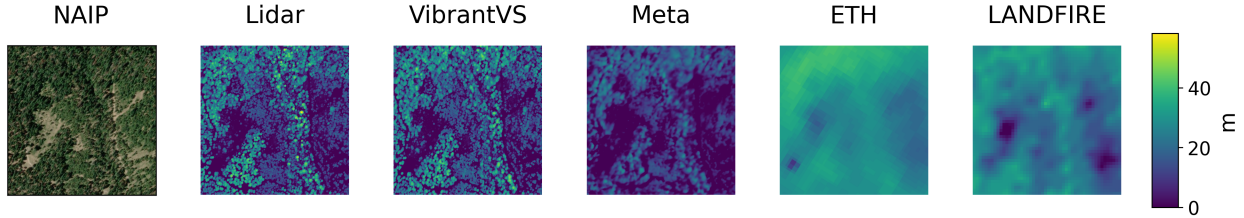


Figure 10: Qualitative evaluation of the various baseline models compared to the original lidar data.

GEDI plots, that may represent sets of conditions that are too limited to create a robust model. Although other factors such as the use of higher resolution NAIP imagery have contributed as well, we attribute most of our performance gains to our robust training dataset and especially to our selection of model improvements for our ViT. [54] have used a U-Net-based approach with the same type of NAIP input data to estimate canopy heights, but evaluated the performance only in California and therefore we could not include them in this analysis.

The temporal alignment of our NAIP images is within a single year of the acquisition date of the aerial lidar for the data used to train VibrantVS. However, this is not the case for the other baseline models. They all aim to represent a CHM from the year 2020; however, their source data come from a wider range of acquisition years: Maxar mosaic data from 2018 to 2022 [47], Landsat data from 2016 [49], or Sentinel-2-L2A data from 2020 [23]. The temporal discrepancy with the acquisition years from 2016 to 2021 of the aerial lidar led to larger estimation errors. However, even when we only compare the models with corresponding lidar data from 2019 to 2021, the trend in the difference in MAE numbers is maintained (Fig. A3). This highlights a specific advantage of the use of NAIP imagery as a model input, given NAIP’s three-year-or-less temporal return interval. This cadence across states allows for monitoring of canopy heights following major disturbances and can provide updated information of the forest structure without the cost of lidar acquisition.

VibrantVS utilizes higher resolution source image data from NAIP compared to the other models. A resolution of 0.5 meters provides better granularity of the features within the image and allows us to provide native estimates at 0.5 meters, which aligns with the aerial lidar CHM that we compare against. Meta provides a CHM at 1-meter resolution, ETH at 10 meters, and LANDFIRE at 30 meters. Given our use of nearest-neighbor resampling to compare our baselines versus lidar, we expected high-resolution comparisons to inflate MAE for baseline models due to their lower native resolutions compared to VibrantVS, but this is not the case when observing MAE for aggregations at spatial resolutions at 10 and 30 meters. When we compare all models at 10 and 30-meter resolutions to lidar CHM at these same resolutions, the trend in differences of overall median MAE is maintained relative to the 0.5-meter results (Fig. 12).

The coarser resolution of the ETH and LANDFIRE models restricts their use to coarse-level applications, for which the trends in overestimation and underestimation at different tree heights could be accounted for with correction factors by height bins. The high-resolution of the VibrantVS model provides the opportunity to generate downstream forest structure products such as Tree Approximate Object (TAO) segmentation [20]. The spatial resolution of a CHM is a critical factor in accurately segmenting individual trees, which often serve as inputs for various forest management activities. Higher resolutions, such as 0.5 meters, can provide detailed canopy representations that a 1-meter pixel resolution model might not capture, leading to less precise segmentation [45]. Additionally, the CHM rasters can serve as input to wildfire spread models, allowing practitioners

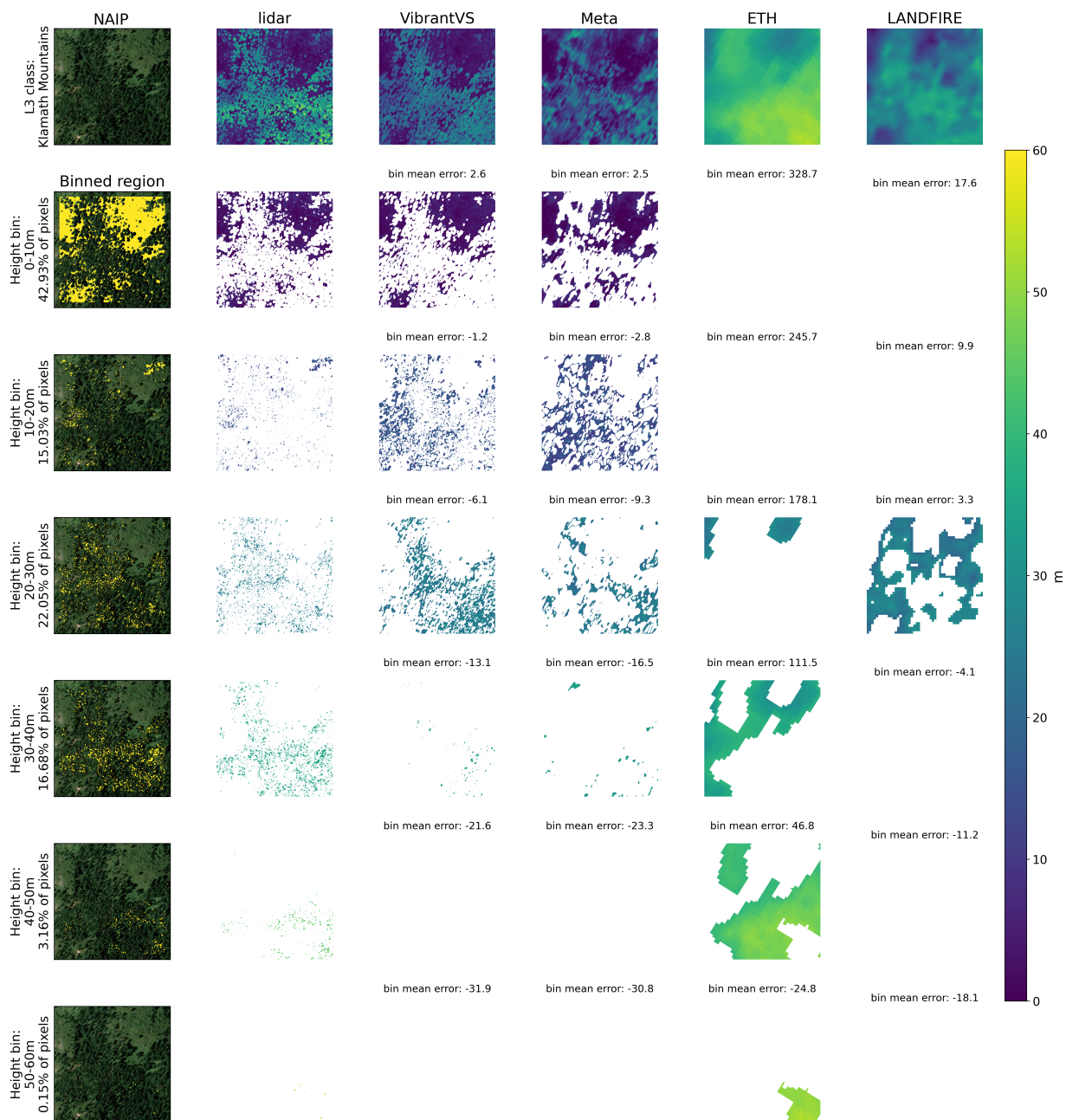


Figure 11: Comparison of model performance at different height class bins.

to better capture discontinuities in fuels that may slow or stop fire progression [36].

From our analysis we determine that the following improvements can be made in future research:

1. More refinements can be made to the evaluations of the lowest height bin. MAE values are higher in this category because the spatial footprint of tree crowns appear larger in NAIP data compared to lidar-based tree crowns. This aerial image-based effect causes the VibrantVS

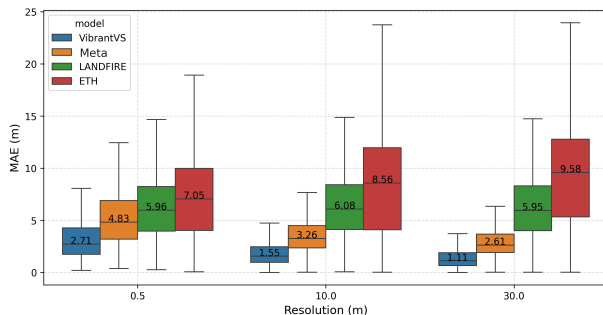


Figure 12: Comparison of model performance at varying resolutions with the target lidar data resampled with averaging method. Median MAE values annotated in box whisker plots.

model to infer a wider canopy crown that results in an overestimation of values where the lidar data are closer to 0. If we use the block metrics of Tolan et al. [47], rather than the pixel-wise metrics of Lang et al. [23], then we expect the lowest bin error of overestimation to disappear.

2. More importantly, we have to address the underestimation of height among trees that are taller than 35 meters, and especially trees taller than 50 meters. There is an imbalance in the number of training samples of tall trees. Trees taller than 50 meters represent less than 0.5% of our training data. We are undertaking a specific retraining exercise to address this underestimation and to compensate for the label imbalance.
3. We would like to integrate topography data into our model, as we suspect that this could improve accuracy, especially on steep slopes.
4. We are also planning to expand our range of applications to more ecoregions, especially in the central and eastern United States. This would allow us to include additional tree species and also shrub vegetation types and to evaluate CHMs at heights lower than 2 meters.

6 Conclusion

This paper presents a comprehensive analysis of three baseline CHM models and our custom vision transformer model (VibrantVS), which is based on NAIP imagery. Our findings indicate that, while each model has its strengths, their success varies significantly between different ecoregions. VibrantVS outperforms all three baseline models in both accuracy and precision across the majority of ecoregions and ranges of canopy heights. It comes with the distinct advantage of being able to produce a very high resolution (0.5 meters) CHM and can be updated with a cadence of three years or less. Additionally, VibrantVS is based on publicly and freely available data in the United States and can be an alternative to collecting aerial lidar at high costs.

The very high-resolution CHMs from VibrantVS can be used in the TAO segmentation process, which allows for the downstream estimation of key forest-structure variables, such as trees per acre, basal area, timber volume, canopy base height, and biomass. These variables are essential for decision making in forestry and land management. These derived variables can also be integrated into existing fire models to predict fire risk and behavior at high resolution.

Acknowledgments

The authors would like to thank Leo Tsourides and Derek Young for their support and consulting in this research. Additional gratitude is extended to Ian Reese, Fabian Döweler, Finlay Thompson, and the rest of the Dragonfly Data Science team for initial proof-of-concept work. The authors thank NASA and USDA for their support. Luke J. Zachmann was funded in part by USDA grant number NR233A750004G042, subaward number 5; Tony Chang, Andreas Gros, and Vincent A. Landau were funded in part by NASA grant number 80NSSC22K1734.

References

- [1] J. T. Abatzoglou and A. P. Williams. Impact of anthropogenic climate change on wildfire across western us forests. *Proceedings of the National Academy of sciences*, 113(42):11770–11775, 2016.
- [2] J. Ainslie, J. Lee-Thorp, M. de Jong, Y. Zemlyanskiy, F. Lebrón, and S. Sanghai. Gqa: Training generalized multi-query transformer models from multi-head checkpoints. *arXiv preprint arXiv:2305.13245*, 2023.
- [3] H.-E. Andersen, R. J. McGaughey, and S. E. Reutebuch. Estimating forest canopy fuel parameters using lidar data. *Remote sensing of Environment*, 94(4):441–449, 2005.
- [4] AWS Open Data Registry. Naip: National agriculture imagery program, 2024. URL <https://registry.opendata.aws/naip/>. Accessed: 2024-09-26.
- [5] M. Beland, G. Parker, B. Sparrow, D. Harding, L. Chasmer, S. Phinn, A. Antonarakis, and A. Strahler. On promoting the use of lidar systems in forest ecosystem research. *Forest Ecology and Management*, 450:117484, 2019.
- [6] S. F. Bhat, R. Birkl, D. Wofk, P. Wonka, and M. Müller. Zoedepth: Zero-shot transfer by combining relative and metric depth. *arXiv preprint arXiv:2302.12288*, 2023.
- [7] T. Dao. Flashattention-2: Faster attention with better parallelism and work partitioning. *arXiv preprint arXiv:2307.08691*, 2023.
- [8] T. Darcet, M. Oquab, J. Mairal, and P. Bojanowski. Vision transformers need registers. *arXiv preprint arXiv:2309.16588*, 2023.
- [9] A. Defazio, H. Mehta, K. Mishchenko, A. Khaled, A. Cutkosky, et al. The road less scheduled. *arXiv preprint arXiv:2405.15682*, 2024.
- [10] T. Dettmers, M. Lewis, S. Shleifer, and L. Zettlemoyer. 8-bit optimizers via block-wise quantization. *CoRR*, abs/2110.02861, 2021. URL <https://arxiv.org/abs/2110.02861>.
- [11] M. Drusch, U. Del Bello, S. Carlier, O. Colin, V. Fernandez, F. Gascon, B. Hoersch, C. Isola, P. Laberinti, P. Martimort, et al. Sentinel-2: Esa’s optical high-resolution mission for gmes operational services. *Remote sensing of Environment*, 120:25–36, 2012.
- [12] R. Dubayah, J. Armston, S. P. Healey, J. M. Bruening, P. L. Patterson, J. R. Kellner, L. Duncanson, S. Saarela, G. Ståhl, Z. Yang, et al. Gedi launches a new era of biomass inference from space. *Environmental Research Letters*, 17(9):095001, 2022.

- [13] R. O. Dubayah and J. B. Drake. Lidar remote sensing for forestry. *Journal of forestry*, 98(6): 44–46, 2000.
- [14] Earth Resources Observation And Science (EROS) Center. National Agriculture Imagery Program (NAIP), 2017. URL https://www.usgs.gov/centers/eros/science/usgs-eros-archive-aerial-photography-national-agriculture-imagery-program-naip?qt-science_center_objects=0#qt-science_center_objects.
- [15] ETH Zurich. Global canopy height map for the year 2020 derived from sentinel-2 and gedi (version 1), 2023. URL <https://doi.org/10.3929/ethz-b-000609802>. ETH Zurich Research Collection.
- [16] A. Ferraz, F. Bretar, S. Jacquemoud, G. Gonçalves, L. Pereira, M. Tomé, and P. Soares. 3d mapping of a multi-layered mediterranean forest using als data. *Remote Sensing of Environment*, 121:210–223, 2012. doi: 10.1016/j.rse.2012.01.020.
- [17] S. E. Franklin, M. B. Lavigne, M. A. Wulder, and G. B. Stenhouse. Change detection and landscape structure mapping using remote sensing. *The Forestry Chronicle*, 78(5):618–625, 2002.
- [18] P. F. Hessburg, J. K. Agee, and J. F. Franklin. Dry forests and wildland fires of the inland northwest usa: contrasting the landscape ecology of the pre-settlement and modern eras. *Forest Ecology and management*, 211(1-2):117–139, 2005.
- [19] K. M. Hoffman, E. L. Davis, S. B. Wickham, K. Schang, A. Johnson, T. Larking, P. N. Lauriault, N. Quynh Le, E. Swerdfager, and A. J. Trant. Conservation of earth’s biodiversity is embedded in indigenous fire stewardship. *Proceedings of the National Academy of Sciences*, 118(32):e2105073118, 2021.
- [20] S. M. A. Jeronimo, V. R. Kane, D. J. Churchill, R. J. McGaughey, and J. F. Franklin. Applying lidar individual tree detection to management of structurally diverse forest landscapes. *Journal of Forestry*, 116(4):336–346, June 2018. ISSN 1938-3746. doi: 10.1093/jofore/fvy023. URL <http://dx.doi.org/10.1093/jofore/fvy023>.
- [21] H. A. Kramer, B. M. Collins, M. Kelly, and S. L. Stephens. Quantifying ladder fuels: A new approach using lidar. *Forests*, 5(6):1432–1453, 2014.
- [22] M. L. Lane, T. W. Swetnam, and T. Oki. Fuel models and landfire: Standardizing inputs for fire simulation. *International Journal of Wildland Fire*, 20(7):845–856, 2011. doi: 10.1071/WF10158. URL <https://doi.org/10.1071/WF10158>.
- [23] N. Lang, W. Jetz, K. Schindler, and J. D. Wegner. A high-resolution canopy height model of the earth. *Nature Ecology & Evolution*, 7(11):1778–1789, 2023.
- [24] M. A. Lefsky, W. B. Cohen, G. G. Parker, and D. J. Harding. Lidar remote sensing for ecosystem studies. *BioScience*, 52(1):19–30, 2002.
- [25] S. Li, M. Brandt, R. Fensholt, A. Kariryaa, C. Igel, F. Gieseke, T. Nord-Larsen, S. Oehmcke, A. H. Carlsen, S. Junttila, et al. Deep learning enables image-based tree counting, crown segmentation, and height prediction at national scale. *PNAS nexus*, 2(4):pgad076, 2023.

- [26] Z. Liu, H. Hu, Y. Lin, Z. Yao, Z. Xie, Y. Wei, J. Ning, Y. Cao, Z. Zhang, L. Dong, et al. Swin transformer v2: Scaling up capacity and resolution. In *Proceedings of the IEEE/CVF conference on computer vision and pattern recognition*, pages 12009–12019, 2022.
- [27] Maxar Technologies. Maxar vivid2 mosaic imagery data. <https://developers.maxar.com/docs/streaming-basemap>, 2024. Accessed August 8, 2024.
- [28] J. E. Means, S. A. Acker, D. J. Harding, J. B. Blair, M. A. Lefsky, W. B. Cohen, M. E. Harmon, and W. A. McKee. Use of large-footprint scanning airborne lidar to estimate forest stand characteristics in the western cascades of oregon. *Remote sensing of environment*, 67(3): 298–308, 1999.
- [29] Meta and World Resources Institute (WRI). High resolution canopy height maps (chm). <https://registry.opendata.aws/dataforgood-fb-forests>, 2024.
- [30] M. A. Moritz, E. Batllori, R. A. Bradstock, A. M. Gill, J. Handmer, P. F. Hessburg, J. Leonard, S. McCaffrey, D. C. Odion, T. Schoennagel, et al. Learning to coexist with wildfire. *Nature*, 515(7525):58–66, 2014.
- [31] J. H. Olszewski and J. D. Bailey. Lidar as a tool for assessing change in vertical fuel continuity following restoration. *Forests*, 13(4):503, 2022.
- [32] J. M. Omernik and G. E. Griffith. Ecoregions of the conterminous united states: evolution of a hierarchical spatial framework. *Environmental management*, 54:1249–1266, 2014.
- [33] S. C. Popescu and R. H. Wynne. Seeing the trees in the forest. *Photogrammetric Engineering & Remote Sensing*, 70(5):589–604, 2004.
- [34] R. Ranftl, K. Lasinger, D. Hafner, K. Schindler, and V. Koltun. Towards robust monocular depth estimation: Mixing datasets for zero-shot cross-dataset transfer. *IEEE transactions on pattern analysis and machine intelligence*, 44(3):1623–1637, 2020.
- [35] D. Riaño, E. Meier, B. Allgöwer, E. Chuvieco, and S. L. Ustin. Modeling airborne laser scanning data for the spatial generation of critical forest parameters in fire behavior modeling. *Remote Sensing of Environment*, 86(2):177–186, 2003.
- [36] T. Ritu, H. James, W. L. ad Reinke Karin, and J. Simon. Effect of fuel spatial resolution on predictive wildfire models. *International Journal of Wildland Fire*, 30:776–789, 2021. doi: 10.1071/WF20192. URL <https://doi.org/10.1071/WF20192>.
- [37] M. G. Rollins. Landfire: a nationally consistent vegetation, wildland fire, and fuel assessment. *International Journal of Wildland Fire*, 18(3):235–249, 2009.
- [38] M. G. Rollins, R. E. Keane, Z. Zhu, and J. P. Menakis. An overview of the landfire prototype project. In: *Rollins, Matthew G.; Frame, Christine K., tech. eds. 2006. The LANDFIRE Prototype Project: nationally consistent and locally relevant geospatial data for wildland fire management Gen. Tech. Rep. RMRS-GTR-175. Fort Collins: US Department of Agriculture, Forest Service, Rocky Mountain Research Station. p. 5-43, 175, 2006.*

- [39] J.-R. Roussel, D. Auty, N. C. Coops, P. Tompalski, T. R. Goodbody, A. S. Meador, J.-F. Bourdon, F. de Boissieu, and A. Achim. lidar: An r package for analysis of airborne laser scanning (als) data. *Remote Sensing of Environment*, 251:112061, 2020. ISSN 0034-4257. doi: 10.1016/j.rse.2020.112061. URL <https://www.sciencedirect.com/science/article/pii/S0034425720304314>.
- [40] N. Shazeer. Glu variants improve transformer. *arXiv preprint arXiv:2002.05202*, 2020.
- [41] C. A. Silva, A. T. Hudak, L. A. Vierling, E. L. Loudermilk, J. J. O’Brien, J. K. Hiers, S. B. Jack, C. Gonzalez-Benecke, H. Lee, M. J. Falkowski, et al. Imputation of individual longleaf pine (*pinus palustris* mill.) tree attributes from field and lidar data. *Canadian journal of remote sensing*, 42(5):554–573, 2016.
- [42] S. L. Steenburgh and K. R. Schmid. Landfire program: Fuel data for fire and resource management planning. *Fire Ecology*, 8(2):89–96, 2012. doi: 10.4996/fireecology08189. URL <https://doi.org/10.4996/fireecology08189>.
- [43] C. S. Stevens-Rumann, K. B. Kemp, P. E. Higuera, B. J. Harvey, M. T. Rother, D. C. Donato, P. Morgan, and T. T. Veblen. Evidence for declining forest resilience to wildfires under climate change. *Ecology letters*, 21(2):243–252, 2018.
- [44] L. J. Sugarbaker, E. W. Constance, H. K. Heidemann, A. L. Jason, V. Lukas, D. L. Saghy, and J. M. Stoker. The 3d elevation program initiative: a call for action. Technical report, U.S. Geological Survey, 2014.
- [45] R.-L. Team. Lidar data analysis with r: Canopy height models, 2024. URL https://r-lidar.github.io/lidRbook/dsm.html?utm_source=chatgpt.com. Accessed: 2024-12-03.
- [46] K. M. Thibault, C. M. Laney, K. M. Yule, N. M. Franz, and P. M. Mabee. The us national ecological observatory network and the global biodiversity framework: national research infrastructure with a global reach. *Journal of Ecology and Environment*, 47, 2023.
- [47] J. Tolan, H.-I. Yang, B. Nosarzewski, G. Couairon, H. V. Vo, J. Brandt, J. Spore, S. Majumdar, D. Haziza, J. Vamaraju, et al. Very high resolution canopy height maps from RGB imagery using self-supervised vision transformer and convolutional decoder trained on aerial lidar. *Remote Sensing of Environment*, 300:113888, 2024.
- [48] U.S. Forest Service. Initial landscape investments to support the national wild-fire crisis strategy, 2022. URL <https://www.fs.usda.gov/sites/default/files/WCS-Initial-Landscape-Investments.pdf>. U.S. Department of Agriculture.
- [49] U.S. Geological Survey. Landfire fuels - forest canopy height, 2022. URL <https://www.landfire.gov/fuel/ch>. Accessed: 2024-04-27.
- [50] U.S. Geological Survey. WESM Data Dictionary. <https://www.usgs.gov/ngp-standards-and-specifications/wesm-data-dictionary/>, 2024. [Online; accessed 7-August-2024].
- [51] R. Valbuena, B. O’Connor, F. Zellweger, W. Simonson, P. Vihervaara, M. Maltamo, C. A. Silva, D. R. A. d. Almeida, F. Danks, F. Morsdorf, et al. Standardizing ecosystem morphological traits from 3d information sources. *Trends in Ecology & Evolution*, 35(8):656–667, 2020.

- [52] M. Van Leeuwen and M. Nieuwenhuis. Retrieval of forest structural parameters using lidar remote sensing. *European Journal of Forest Research*, 129:749–770, 2010.
- [53] K. T. Vierling, L. A. Vierling, W. A. Gould, S. Martinuzzi, and R. M. Clawges. Lidar: shedding new light on habitat characterization and modeling. *Frontiers in Ecology and the Environment*, 6(2):90–98, 2008.
- [54] F. H. Wagner, S. Roberts, A. L. Ritz, G. Carter, R. Dalagnol, S. Favrichon, M. C. Hirye, M. Brandt, P. Ciais, and S. Saatchi. Sub-meter tree height mapping of california using aerial images and lidar-informed u-net model. *Remote Sensing of Environment*, 305:114099, 2024. ISSN 0034-4257. doi: <https://doi.org/10.1016/j.rse.2024.114099>. URL <https://www.sciencedirect.com/science/article/pii/S003442572400110X>.
- [55] K. F. Watts, D. W. Koehler, D. Todd, and N. Gillett. Integration of landfire data into fire modeling: Enhancing accuracy and consistency. *Journal of Applied Meteorology and Climatology*, 56(9):2017JA024010, 2017. doi: 10.1175/JAMC-D-16-0253.1. URL <https://doi.org/10.1175/JAMC-D-16-0253.1>.
- [56] A. L. Westerling. Increasing western US forest wildfire activity: sensitivity to changes in the timing of spring. *Philosophical Transactions of the Royal Society B: Biological Sciences*, 371(1696):20150178, June 2016. doi: 10.1098/rstb.2015.0178. URL <https://royalsocietypublishing.org/doi/full/10.1098/rstb.2015.0178>. Publisher: Royal Society.
- [57] J. C. White, N. C. Coops, M. A. Wulder, M. Vastaranta, T. Hilker, and P. Tompalski. Remote sensing technologies for enhancing forest inventories: A review. *Canadian Journal of Remote Sensing*, 42(5):619–641, 2016.
- [58] M. A. Wulder, C. W. Bater, N. C. Coops, T. Hilker, and J. C. White. The role of lidar in sustainable forest management. *The forestry chronicle*, 84(6):807–826, 2008.
- [59] B. Zhang and R. Sennrich. Root mean square layer normalization. *Advances in Neural Information Processing Systems*, 32, 2019.

A Appendix

A.1 Additional Tables and Figures

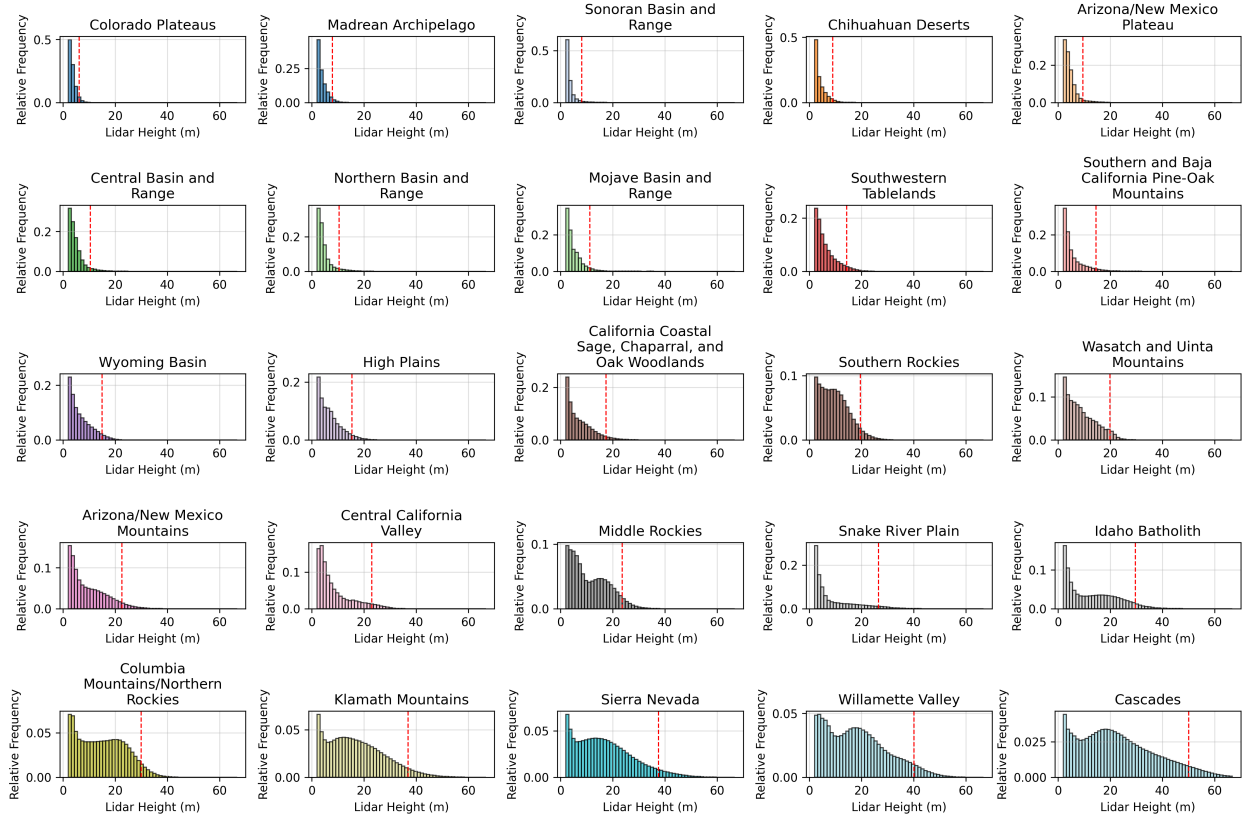


Figure A1: Lidar sample pixel-wise height distributions within each of the EPA Level 3 ecoregions. Red dashed line represents the 95th percentile of the height distribution.

A.2 Error metrics

1. Mean Absolute Error (MAE)

$$\text{MAE} = \frac{1}{n} \sum_{i=1}^n |y_i - \hat{y}_i|$$

2. Block- R^2

$$R_{\text{block}}^2 = 1 - \frac{\sum_{b=1}^B \sum_{i \in b} (y_i - \hat{y}_i)^2}{\sum_{b=1}^B \sum_{i \in b} (y_i - \bar{y}_b)^2}$$

Where B is the number of blocks, y_b is the ground truth value in block b , \hat{y}_b the model estimate for block b , and \bar{y}_b is the mean of the ground-truth values in block b .

Model	Spatial Resolution	Spatial Extent	Temporal Coverage	Model Type	Predictor Data	Label Data
VibrantVS	0.5-meter	Western United States	2014-2021	Multi-task vision transformer	4-band NAIP imagery	USGS 3DEP aerial lidar
Meta [47]	1-meter	Global	2020	Encoder, dense prediction transformer, correction and rescaling network	Maxar Vivid2 0.5-meter resolution mosaics	NEON aerial lidar CHMs, GEDI data, and a labeled 9000 tile tree/no tree segmentation dataset
LAND FIRE [37]	30-meter	United States	2016, 2020, 2022, 2023	Regression-tree based methods	Spectral information from Landsat, landscape features such as topography, and biophysical information	Field-measured height
ETH [23]	10-meter	Global	2020	Deep learning ensemble	Sentinel-2-L2A multi-spectral imagery, sin-cos embeddings of longitudinal coordinates	Sparse GEDI lidar data

Table A1: Summary of CHM models, spatial resolutions, predictor data, and label data.

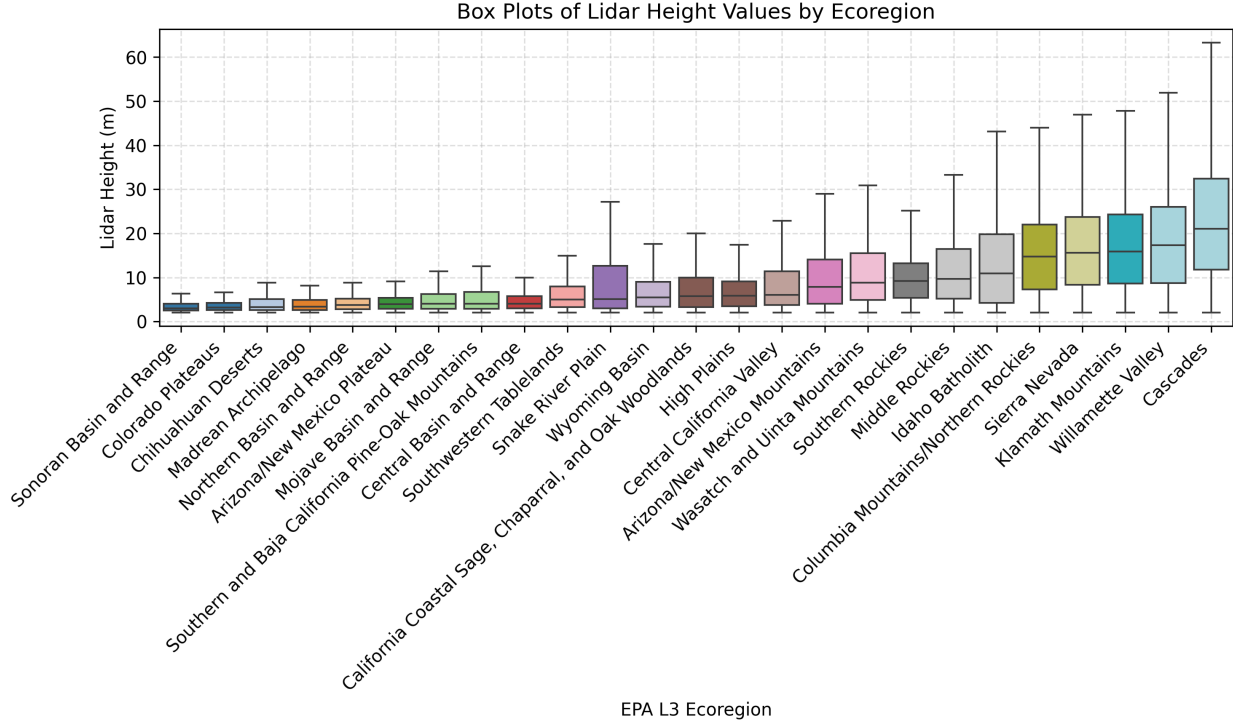


Figure A2: Lidar sample tile height box plots within each EPA Level 3 ecoregion.

3. Root Mean Square Error (RMSE)

$$\text{RMSE} = \sqrt{\frac{1}{n} \sum_{i=1}^n (y_i - \hat{y}_i)^2}$$

4. Mean Error (ME)

$$\text{ME} = \frac{1}{n} \sum_{i=1}^n (\hat{y}_i - y_i)$$

5. Edge Error Metric (EE)

$$\text{EE} = \frac{1}{n} \sum_{i=1}^n |E(\hat{y}_i) - E(y_i)|$$

Where $E(\cdot)$ represents Sobel edge detection operation on the data (also compare Tolan et al. (2024)).

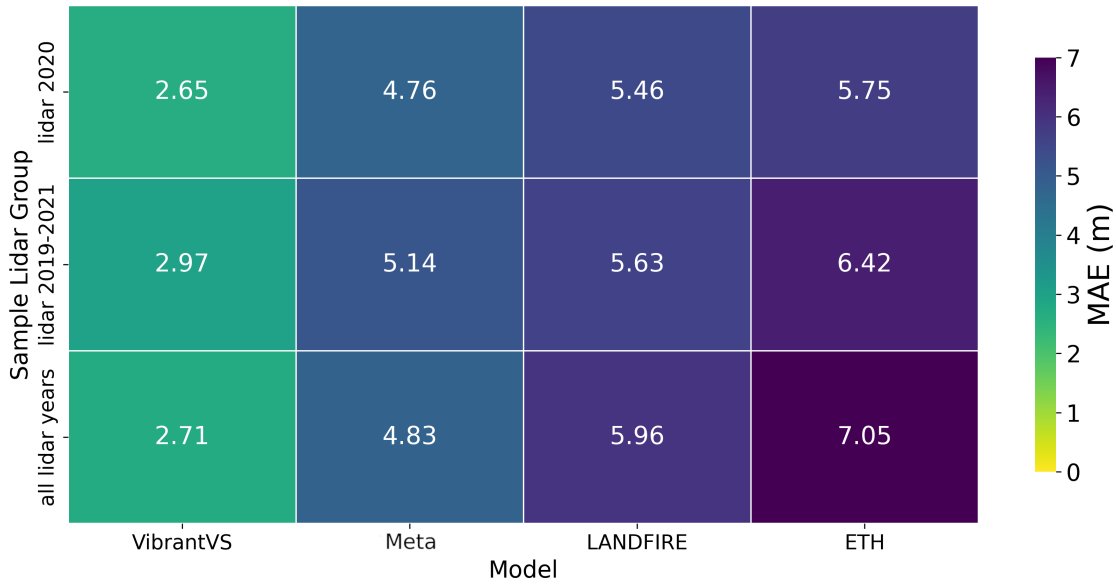
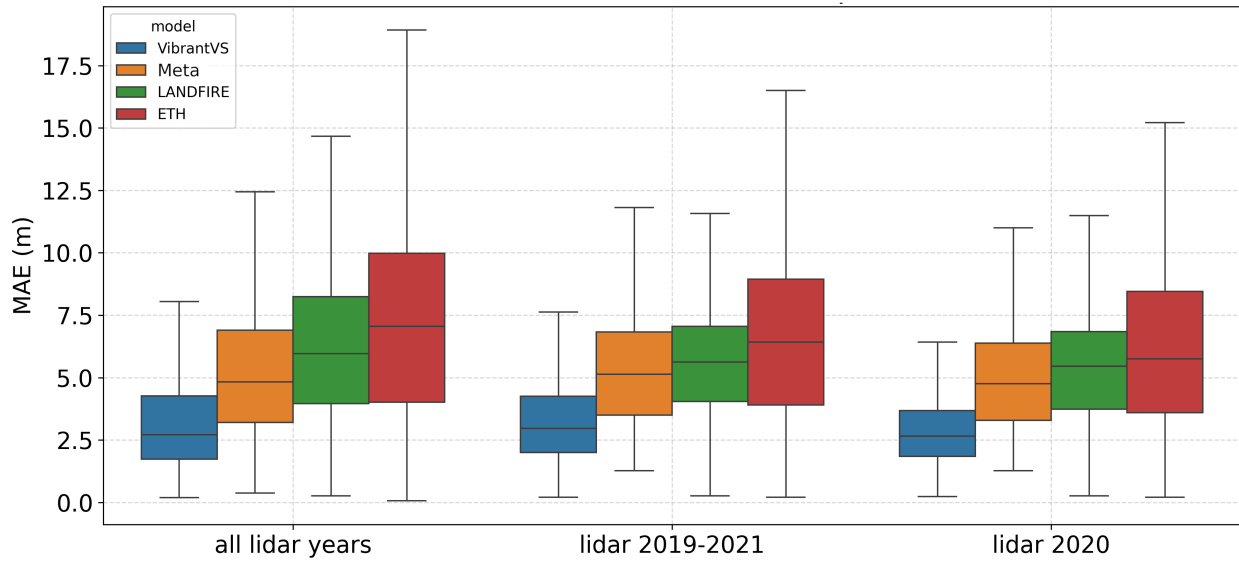


Figure A3: Comparison of model performance at different year groups of lidar acquisition determine temporal mismatch error.